SLAS Discovery 29 (2024) 100154

Contents lists available at ScienceDirect

SLAS Discovery

journal homepage: www.elsevier.com/locate/slasd

Full Length Article

Aldehyde Dehydrogenase 2 (ALDH2): A novel sorafenib target in hepatocellular carcinoma unraveled by the proteome-wide cellular thermal shift assay

Inês C. Ferreira [a,1], Estefania Torrejón [a,b,1], Bernardo Abecasis [a], Bruno M. Alexandre [a,b], Ricardo A. Gomes [a,b], Chris Verslype [c], Jos van Pelt [d], Ana Barbas [a,e], Daniel Simão [a], Tiago M. Bandeiras [a,b], Alessio Bortoluzzi [a,b,**], Sofia P. Rebelo [a,*]

[a] iBET, Instituto de Biologia Experimental e Tecnológica, Apartado 12, 2781-901 Oeiras, Portugal
[b] ITQB, ITQB-NOVA, Instituto de Tecnologia Química e Biológica António Xavier, Universidade Nova de Lisboa, Oeiras, Portugal
[c] Department of Gastroenterology and Hepatology, KU Leuven, Leuven, Belgium
[d] Department of Oncology, Laboratory of Clinical Digestive Oncology, KU, Leuven, Belgium
[e] Bayer Portugal, Carnaxide, Portugal

ARTICLE INFO

Keywords:
ALDH2
Sorafenib
HCC
CETSA-MS
Target validation

ABSTRACT

Sorafenib is a multikinase inhibitor indicated for first-line treatment of unresectable hepatocellular carcinoma. Despite its widespread use in the clinic, the existing knowledge of sorafenib mode-of-action remains incomplete. To build upon the current understanding, we used the Cellular Thermal Shift Assay (CETSA) coupled to Mass Spectrometry (CETSA-MS) to monitor compound binding to its target proteins in the cellular context on a proteome-wide scale. Among the potential sorafenib targets, we identified aldehyde dehydrogenase 2 (ALDH2), an enzyme that plays a major role in alcohol metabolism. We validated the interaction of sorafenib with ALDH2 by orthogonal methods using pure recombinant protein, proving that this interaction is not mediated by other cellular components. Moreover, we showed that sorafenib inhibits ALDH2 activity, supporting a functional role for this interaction. Finally, we were able to demonstrate that both ALDH2 protein expression and activity were reduced in sorafenib-resistant cells compared to the parental cell line. Overall, our study allowed the identification of ALDH2 as a novel sorafenib target and sheds light on its potential role in both hepatocellular carcinoma and sorafenib resistance condition.

1. Introduction

Liver cancer is the fourth leading cause of cancer-related deaths worldwide and hepatocellular carcinoma (HCC) is the most predominant type of liver cancer, accounting for more than 90 % of the cases [1]. The first-line treatment for patients with advanced HCC is the multikinase inhibitor sorafenib, constituting one of the most effective single-drug therapies for HCC [2,3].

Sorafenib acts as an inhibitor of tumor cell proliferation and tumor angiogenesis, also inducing apoptosis in a broad range of tumor models [4–6], including in HCC [7]. This small molecule was first described as an inhibitor of the serine-threonine kinases Raf-1 and B-Raf of the Ras/Raf/MEK/ERK signaling pathway that regulates fundamental cell functions such as growth, survival, and differentiation [4,5]. It was then shown that sorafenib can also inhibit tyrosine kinase receptors, namely vascular-endothelial growth factor receptors (VEGFRs)−1/2/3, platelet-derived growth factor receptor β (PDGFR-β), hepatocyte factor receptor (c-Kit) and FMS-like tyrosine kinase (FLT-3), which are key players in angiogenesis [5]. Further studies focused on better understanding sorafenib mechanism of action, and several of them suggest that anti-tumor effects of this small molecule might be mediated by other pathways. This includes inhibition of mitogen-activated protein kinase 14 (MAPK14) phosphorylation [8], reactive oxygen species (ROS) production [9] and ferroptosis [10].

* Corresponding author.
** Co-corresponding author at: iBET, Instituto de Biologia Experimental e Tecnológica, Apartado 12, 2781-901 Oeiras, Portugal.
E-mail addresses: alessio.bortoluzzi@ibet.pt (A. Bortoluzzi), sofiarebelo@ibet.pt (S.P. Rebelo).
[1] These authors contributed equally.

https://doi.org/10.1016/j.slasd.2024.100154
Received 20 December 2023; Received in revised form 13 March 2024; Accepted 19 March 2024
Available online 21 March 2024

Together these studies have shown that sorafenib has a multitude of interacting partners much broader than initially described. Increased knowledge on the sorafenib target landscape is key to understand the emergence of resistance during treatment and potentially shed light on how to overcome it. Over the last years, omics technologies have emerged as relevant tools to uncover the complexity of sorafenib inhibitory mechanisms, particularly in HCC, having contributed to identify additional direct binders, including non-kinase targets. This comprises technologies such as DNA microarray [11], RNA-Seq analysis [12], Tandem Mass Tag (TMT)-based quantitative proteomics [13] and PROTAC-based quantitative proteomics [14]. In the present work, we propose to use CETSA-MS to identify proteins engaged by sorafenib in a human hepatoma cell model system. CETSA is a well-established tool to assess target engagement in both in-lysate and in-cell contexts [15]. This method is based on the thermal stability changes that a ligand, including small molecules like sorafenib, causes when it binds to a target protein [16]. CETSA-MS is an updated format of this technology in which protein detection is performed by multiplexed quantitative mass spectrometry (MS), enabling a proteome-wide monitoring of changes in thermal stability induced by the compound under investigation, with a potential of finding unknown targets [17]. Among the potential targets identified in our proteomics study, ALDH2 was identified as a novel sorafenib target and its engagement was validated by orthogonal methods. ALDH2 is a mitochondrial enzyme strongly related to liver function. This protein is a key enzyme in alcohol metabolism with a major role in the oxidation of both endogenous and exogenous aldehydes into their corresponding acids [18]. Many studies have shown that ALDH2 has an important role in a variety of human pathologies [19], including cancer [20–22].

The present study unravels for the first time ALDH2 as a novel sorafenib target in hepatocellular carcinoma and reports the identification of sorafenib-interacting proteins by CETSA-MS.

2. Material and methods

2.1. HepG2 cell culture

HepG2 cells (ATCC, HB8065) were maintained at 37 °C and 5 % CO_2 in Dulbecco's Modified Eagle Medium (DMEM), with low glucose, GlutaMAX and pyruvate, and supplemented with 10 % heat-inactivated fetal bovine serum (FBS) and 1 % penicillin-streptomycin (all from Gibco). Two independent HepG2 cultures (both from ATCC) were maintained in two different laboratories. These are referred to as HepG2A and HepG2B. All experiments were performed with HepG2A except otherwise mentioned. Sorafenib-resistant cell lines were generated from the HepG2B cell line by Van Malenstein et al., 2013 [23] and maintained in culture with 6 μM of sorafenib (Tocris Bioscience).

2.2. Preparation of cell lysates

Cell pellets were resuspended in CETSA-MS buffer containing 20 mM HEPES, 138 mM NaCl, 5 mM KCl, 2 mM $CaCl_2$, 1 mM $MgCl_2$, pH 7.4 (according to Chernobrovkin et al., 2020 [24] and Friman et al., 2020 [25]) to a final density of 30×10^6 cells/mL and then lysed with three cycles of freeze-thawing in liquid nitrogen. Lysates were then centrifuged at 16,100 × *g* for 40 min at 4 °C, and the supernatant collected. Final lysate protein concentration was determined using Pierce BCA Protein Assay Kit (Thermo Scientific).

2.3. Thermal profiling in cell lysates

Sorafenib-treated cell lysates were prepared by adding sorafenib to a final concentration of 20 μM in 1 % (v/v) DMSO (Sigma-Aldrich) to the HepG2 lysate. A 1 % (v/v) DMSO vehicle control was prepared in parallel. Compound and vehicle samples were incubated for 1 or 2 h (for ALDH2 and MAPK14, respectively) on ice, divided into aliquots, and heated for 5 min at increasing temperatures (37, 41, 45, 49, 53, 57, 62, 67 °C) in an Applied Biosystems Veriti 96 Well Thermal Cycler (Thermo Scientific). Subsequently, the extract was centrifuged at 25,000 × *g* for 45 min at 4 °C to pellet the aggregated proteins. Supernatants were collected and protein concentration was determined using the Pierce BCA Protein Assay Kit (Thermo Scientific).

2.4. Thermal profiling in intact cells

HepG2 cell suspension at a density of 0.7×10^6 or 3×10^6 cells/mL (for ALDH2 and MAPK14, respectively) was prepared in FBS- and antibiotic-free growth medium (DMEM with low glucose, GlutaMAX and pyruvate). Sorafenib was added to a final concentration of 20 μM in 1 % (v/v) DMSO. A 1 % (v/v) DMSO vehicle control was prepared in parallel. Treated cells were incubated for 1 or 2 h (for ALDH2 and MAPK14, respectively) at 37 °C and 5 % CO_2 with gentle rotation using the mixing cycler Multi Bio RS-24 (Biosan). Cells were centrifuged for 3 min at 300 × *g*, washed and resuspended in CETSA-MS buffer. Each suspension was divided into aliquots and processed for thermal treatment as described for in-lysate experiments. After cell lysis by freeze-thawing, lysates were centrifuged at 16,000 × *g* for 40 min at 4 °C. The supernatants were collected, and protein concentration was determined as described in Section 2.3.

2.5. Isothermal dose response ($ITDR_{CETSA}$)

For $ITDR_{CETSA}$ experiments, sorafenib concentrations used were 100, 66.6, 22.2, 7.3, 2.43, 0.81, 0.27, 0.09, 0.03 and 0.01 μM. A 1 % (v/v) DMSO vehicle control was prepared in parallel. Sorafenib-treated cell lysate aliquots were incubated for 1 or 2 h (for ALDH2 and MAPK14, respectively) on ice and samples were treated as described in Section 2.3 with the exception that the thermal cycler was held at a constant temperature (57 °C for MAPK14 and 53 °C for ALDH2).

2.6. Protein detection by capillary western blot

Protein detection was performed using Jess Simple Western system (ProteinSimple) with the 12–230-kDa Jess separation module. Sample preparation was done according to the manufacturer's instructions. Protein loading conditions were target-dependent: 0.02 mg/mL for ALDH2 and 0.15 mg/mL for MAPK14. The primary antibodies used were anti-p38α (R&D Systems, AF8691) at 1:10 and anti-ALDH2 (Invitrogen, MA517029) at 1:50. Protein quantification was performed using Compass for SW software (version 5.0.0).

2.7. Sample preparation for MS

2.7.1. Sample denaturation, reduction, alkylation and digestion

Cell lysates for MS were prepared as in Sections 2.2 and 2.3. and used at 2 mg/mL. The volume of sample to obtain 150 μg of protein in each temperature point was estimated based on the average of quantification of the 37 °C and 41 °C temperature point samples and volume was constant for all samples, as described in Savitski et al., 2014 [17]. RapiGest SF Surfactant (Waters) in 500 mM of triethylammonium bicarbonate buffer (TEAB) (SCIEX) was added to a final concentration of 0.1 % (v/v). Samples were reduced using tris(2-carboxyethyl)phosphine (TCEP) (SCIEX) to a final concentration of 4.35 mM, vortexed and incubated at 60 °C for 1 hour with shaking. Samples were alkylated adding methyl methanethiosulfonate (MMTS) (SCIEX) to a final concentration of 8.3 mM, vortexed and incubated at RT for 10 min under agitation in the dark. 1 μg of LysC (Promega) in 0.001 % of HCl (Merck KGaA) was added for each 50 μg of protein and samples were incubated at 37 °C for 3 h under agitation. Next, 1 μg of trypsin (Promega) in 0.001 % HCl was added for each 50 μg of protein and samples were incubated at 37 °C for 16 h under agitation. Trifluoroacetic acid (TFA) (Thermo Scientific) was added to a final concentration of 0.5 % to stop digestion,

samples were then incubated at 37 °C for 40 min under agitation and centrifuged at 16,000 × *g* for 10 min at RT. The supernatants were collected and dried out using the Eppendorf Vacufuge Plus Vacuum Concentrator.

2.7.2. Isobaric labelling

Sample labelling using iTRAQ 8-plex kit (SCIEX) was performed according to manufacturer's instructions. Briefly, 12.7 μL of each reagent was added into the respective temperature point (the tag 113 was added on 37 °C, 114 on 41 °C, 115 on 45 °C, 116 on 49 °C, 117 on 53 °C, 118 on 57 °C, 119 on 62 °C and 121 on 67 °C) and incubated for 2 h at RT. pH was monitored using pH strips (Supelco) and adjusted to 7.5–8.5 using TEAB at 500 mM, if required. After labelling, all temperature points from the same sample were pooled together on the same tube. Samples were dried using the Eppendorf Vacufuge Plus Vacuum Concentrator.

2.7.3. Sample pre-fractionation

Pierce High pH Reversed-Phase Peptide Fractionation Kit (Thermo Scientific) was used for off-line sample pre-fractionation. Samples were resuspended in 325 μL of TFA at 0.1 %. Triethylamine (Thermo Scientific) was used at 0.1 % to prepare the acetonitrile (ACN) (Fisher Chemical) solutions. The procedure was done following the manufacturer's recommendations with an optimized ACN gradient for fraction elution. The resulting fractions were dried out using the Eppendorf Vacufuge Plus Vacuum Concentrator and resuspended in 10 μL of 0.1 % formic acid (Fisher Chemicals) for LC-MS analysis.

2.8. LC-MS/MS analysis

2.8.1. Liquid chromatography (LC)

Nano-liquid chromatography-tandem mass spectrometry (nanoLC-MS/MS) analysis was performed on an ekspert NanoLC 425 cHiPLC system coupled with a TripleTOF 6600 with a NanoSpray III source (SCIEX). Peptides were separated through reversed-phase chromatography (RP-LC) in a trap-and-elute mode. Trapping was performed at 2 μl/min with 100 % A (0.1 % formic acid in water, Fisher Chemicals), for 10 min, on a Nano cHiPLC Trap column (200 μm x 0.5 mm, ChromXP C18-CL, 3 μm, 120 Å, SCIEX). Separation was performed at 300 nL/min, on a Nano cHiPLC column (75 μm x 15 cm, ChromXP C18-CL, 3 μm, 120 Å, SCIEX). The 90 min long LC gradient, in which solvent A was 0.1 % formic acid in water (Fisher Chemicals) and solvent B was 0.1 % formic acid in ACN (Fisher Chemicals) was optimized for each one of the fractions.

2.8.2. Data acquisition

Peptides were sprayed into the MS through an uncoated fused-silica PicoTip emitter (360 μm O.D., 20 μm I.D., 10 ± 1.0 μm tip I.D., New Objective). The source parameters were set as follows: 15 GS1, 0 GS2, 30 CUR, 2.5 keV ISVF and 100 ºC IHT. An information dependent acquisition (IDA) method was set with a TOF-MS survey scan of 350–1400 *m/z* for 250 msec. The 50 most intense precursors were selected for subsequent fragmentation and the MS/MS (100–1800 *m/z* for 40 msec each; total cycle time of 2.3 s) were acquired in high sensitivity mode. The selection criteria for parent ions included a charge state between +2 and +5 and counts above a minimum threshold of 125 counts per second. Selected ions were excluded from further MS/MS analysis for 12 s. Fragmentation was performed using a rolling collision energy (CE) adjusted to a spread of 5.

2.9. Peptide and protein identification and quantification

Raw files were processed by the ProteinPilot software (SCIEX, version 5.0) using the Paragon (SCIEX) protein database search algorithm for identification and quantification of iTRAQ samples. The parameters selected were as follows: Sample type: iTRAQ (peptide labeled); Cys-Alkylation: MMTS; Digestion: Trypsin and Lys-C; Instrument: TripleTOF 6600; Special factors: None; Species: None; Quantitate tab: checked; ID Focus: Biological modifications - searches for over 170 potential modifications; Database: 20,210,105_SP_Human_20394entries.fasta (Uniprot); Search Effort: Thorough, FDR Analysis: Yes; User Modified Parameters Files: No. Moreover, a stringent cut-off threshold with total unused score >1.3 was adopted as the qualification criteria, which corresponds to a protein confidence level of >95 % and a false discovery rate (FDR) of 0.33 %.

2.10. Melting curves generation and target selection

The melting curves were fitted using the R package thermal proteome profiling (TPP) by Childs et al., 2020 [26] (R version 4.0.3 and TPP package version 3.18.0). Only proteins presenting quantification for at least three temperature points were considered for the melting curve analysis. The TPP workflow was run with the default settings, except for a variation on the Selection of Proteins for Normalization Requirements, which were modified for the presence of only 8 temperature points (instead of the standard 10), keeping the default criteria in which the protein ratios between the highest temperature point (67 °C) and the lowest (37 °C) must fit in within a 0–0.2 range, the ratio for the second highest (62 °C) in between 0 and 0.3 and for the fourth highest (53 °C) in between of 0.4–0.6. To filter possible targets for sorafenib, the following conditions were used: i) The difference in melting temperatures of the target protein between control and sorafenib-treated samples (ΔT_m) must be higher than +2 °C or lower than −2 °C (for stabilization or destabilization, respectively) in at least 3 of the 4 replicates, ii) The average ΔT_m value must be at least four times higher than the standard deviation of the ΔT_m across the four replicates iii) R^2 higher than 0.8 and p-values lower than 0.3. After filtering, all potential targets were revised manually to discard proteins with irregular curve shapes. Corresponding plots were designed using GraphPad Prism software (version 9.1.1).

2.11. Nano-Differential scanning fluorimetry (DSF)

Nano-DSF experiments were performed on a Prometheus NT.48 instrument (NanoTemper Technologies GmbH). The final samples contained ALDH2 (abcam, ab87415) at 0.1 mg/mL with or without sorafenib at 20 μM. Each sample was prepared in triplicates and incubated on ice for 2 h before loading into high-sensitivity capillaries (NanoTemper Technologies) and placed on the Prometheus NT.48 sample holder. Samples were exposed to a temperature gradient from 20 to 95 °C with a gradient slope of 1 °C per minute. The intrinsic protein fluorescence at 330 and 350 nm were recorded, and the T_m was derived from the 350/330 nm fluorescence ratio. The T_m was calculated as the midpoint of each transition using the PR.ThermControl software (version 2.16).

2.12. 1D ^{19}F nuclear magnetic resonance (NMR) spectroscopy

1D ^{19}F NMR spectra were acquired in an 800 MHz Bruker NMR spectrometer (Avance 800 II+) equipped with a CP2.1 TCI cryoprobe with an acquisition time of 91 ms. All samples were prepared in phosphate-buffered saline solution (PBS) (Merck KGaA) and contained 5 μM sorafenib, 1 % DMSO, 10 % D_2O (Cortecnet) and 10 μM TFA (Thermo Scientific). TFA signal was used to normalize signal intensity across spectra. Three proteins were tested at a final concentration of 1 μM: ALDH2 (abcam, ab87415), Bovine Serum Albumin (BSA) (Thermo Scientific, 23,209) and Cyclophilin D (CypD) (purified in-house).

2.13. ALDH2 protein quantification in HepG2 lysates

HepG2 cell lysates (HepG2A, HepG2B, HepG2S1 and HepG2S3) were prepared and quantified as described in Section 2.2. Final lysate concentration was adjusted to the same total protein concentration (0.02

mg/mL). Protein detection was performed using Jess Simple Western system (ProteinSimple) with the 12–230-kDa Jess separation module and sample preparation was done according to the manufacturer's instructions. Primary antibodies used were anti-ALDH2 (Invitrogen, MA517029) at 1:50, anti-β-actin (Sigma, A5441) at 1:20 and anti-vinculin (abcam, ab129002) at 1:50. Protein quantification was performed using Compass for SW software (version 5.0.0). Relative ALDH2 expression was calculated by dividing ALDH2 protein quantification by the corresponding loading control (β-actin or vinculin) quantification for each sample.

2.14. ALDH2 activity assay

ALDH2 activity was measured in HepG2 cell lysates (HepG2A, HepG2B, HepG2S1 and HepG2S3) using the Mitochondrial Aldehyde Dehydrogenase Activity Assay Kit (abcam, ab115348) according to the manufacturer's protocol. Cell lysates were prepared and quantified as described in Section 2.2, used at a final concentration of 0.5 mg/mL and incubated with DMSO 10 %, sorafenib or disulfiram (Sigma-Aldrich) at 100 μM in 10 % (v/v) DMSO for 15 min at RT before adding the samples to the plate strips. Nicotinamide adenine dinucleotide hydrogen (NADH) production was determined spectrophotometrically by monitoring the absorbance intensity at 450 nm every minute for 1 hour using the SpectraMAX i3x (Molecular Devices) microplate reader. The results refer to NADH production measured at 30 min timepoint. ALDH2 activity was normalized to the HepG2A cell line treated with 10 % DMSO (100 %) and to the assay buffer (0 %) and contains up to four independent cell lysates. Unpaired *t*-tests were used to analyze the data. Statistical analysis was performed using GraphPad Prism software (version 9.1.1).

3. Results

3.1. Sorafenib target engagement profile

CETSA-MS was applied to explore which proteins are targeted by sorafenib in cell lysates of the human HepG2 HCC cell line. Among the 4524 unique proteins identified, we were able to fit the thermal profile of 2455 proteins in both DMSO- and sorafenib-treatment conditions (Fig. 1). Proteins that showed a difference in melting temperature (ΔT_m) between the two treatments higher than +2.0 °C or lower than −2.0 °C, in at least 3 out of 4 replicates and that passed quality and statistical criteria (described in the materials and methods), were selected as potential sorafenib targets. As a result, we identified four proteins that are stabilized by sorafenib − MAPK14, DYLT1, ICAM1 and ALDH2 − with a ΔT_m of +4.0, +3.0, +2.4 and +2.0 °C, respectively. Three proteins were destabilized − PP6R1, TRM6 and RPAC1 − showing a ΔT_m of −2.6, −3.2 and −3.4 °C, respectively (Fig. 1; Supplementary Table 1). Of the seven proteins, MAPK14 was the only previously described sorafenib target [27], serving as a positive control of sorafenib engagement (Fig. 2A). ALDH2 (Fig. 2B) was selected to be further explored as a potential sorafenib target due to its role in HCC. The stabilization of these two targets was confirmed by Classic CETSA, where MAPK14 (Fig. 2C) and ALDH2 (Fig. 2D) showed a ΔT_m of +8.2 °C and +4.5 °C, respectively.

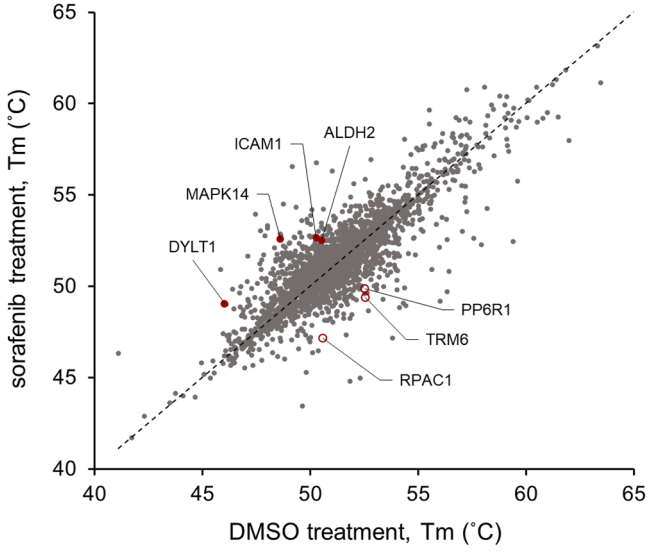

Fig. 1. Scatter plot of T_m determined by CETSA-MS in HepG2 lysates treated with DMSO versus sorafenib. The average T_m (across four independent replicates) determined in DMSO and sorafenib treatments is plotted. Only proteins for which a melting curve could be obtained in at least two replicates for each treatment were plotted (2455). Proteins that passed the quality and statistical criteria to be considered potential sorafenib targets are highlighted in red. Filled circles indicate proteins stabilized while empty circles indicate proteins destabilized by sorafenib.

To investigate whether sorafenib engagement for both identified targets could be confirmed in cellular context, Classic CETSA was performed with intact HepG2 cells instead of lysates. A stabilization of +5.4 °C was obtained for MAPK14 (Fig. 3A), while a thermal shift of +3.1 °C was observed for ALDH2 (Fig. 3B). Additionally, we evaluated the dose-response of sorafenib engagement in cell lysates for both targets by isothermal dose response ($ITDR_{CETSA}$) [15]. In the $ITDR_{CETSA}$, the lysate is exposed to increasing compound concentrations while temperature is kept constant at the T_m selected for each target. For both targets there is a clear drug dose-dependent response resulting in an EC_{50} of 5.3 μM for MAPK14 (Fig. 3C) and 3.5 μM for ALDH2 (Fig. 3D).

3.2. Biophysical characterization of sorafenib binding to ALDH2

To confirm sorafenib binding to ALDH2 and investigate if this is a direct interaction, we used pure recombinant ALDH2 in DSF experiments. ALDH2 showed a single melting transition with a T_m of 54.3 °C. Following incubation with sorafenib a clear positive shift can be observed with a ΔT_m of +5.0 °C in ALDH2 thermal stability (Fig. 4A). To further validate the binding with an orthogonal technique we took advantage of the presence of a trifluoromethyl (CF_3) group in sorafenib molecular structure and resorted to 1D ^{19}F NMR. A concentration of 5 μM of sorafenib was sufficient to detect fluorine signal that could be clearly distinguished from the background (Fig. 4B). Following the addition of ALDH2, sorafenib signal could no longer be detected, probably because of severe peak broadening, which is one of the expected outcomes when of a fluorine-containing small molecule binds to a larger one such as a protein [28,29] (Fig. 4B). The same effect was observed with the addition of BSA, which was used as positive control (given the documented interaction with sorafenib [30]), but not with the negative control, human CypD, a model-protein studied in our laboratory (Fig. 4B). Overall, these results add further evidence of the interaction between ALDH2 and sorafenib and show that also pure recombinant ALDH2 can bind to sorafenib.

3.3. Effect of sorafenib on ALDH2 functionality

After assessing the binding of sorafenib to ALDH2, we wanted to explore its effect on ALDH2 activity. We first analyzed the protein levels of ALDH2 in a HepG2 cell line and compared it to sorafenib-resistant HepG2 cell lines. These cells lines were generated by Van Malenstein and co-workers [23] upon continuous exposure to sorafenib, resulting in decreased sensitivity to sorafenib (higher IC_{50} comparing to the parental cell line) along with changes in morphology, cell expression and invasive potential. Expression was evaluated using β-actin and vinculin as loading controls, revealing high levels of ALDH2 in HepG2A and HepG2B cells. Importantly, we observed a decrease in ALDH2 levels in both resistant cell lines (HepG2S1 and HepG2S3) when compared to the sorafenib-sensitive cell lines (HepG2A and HepG2B) with a fold-change

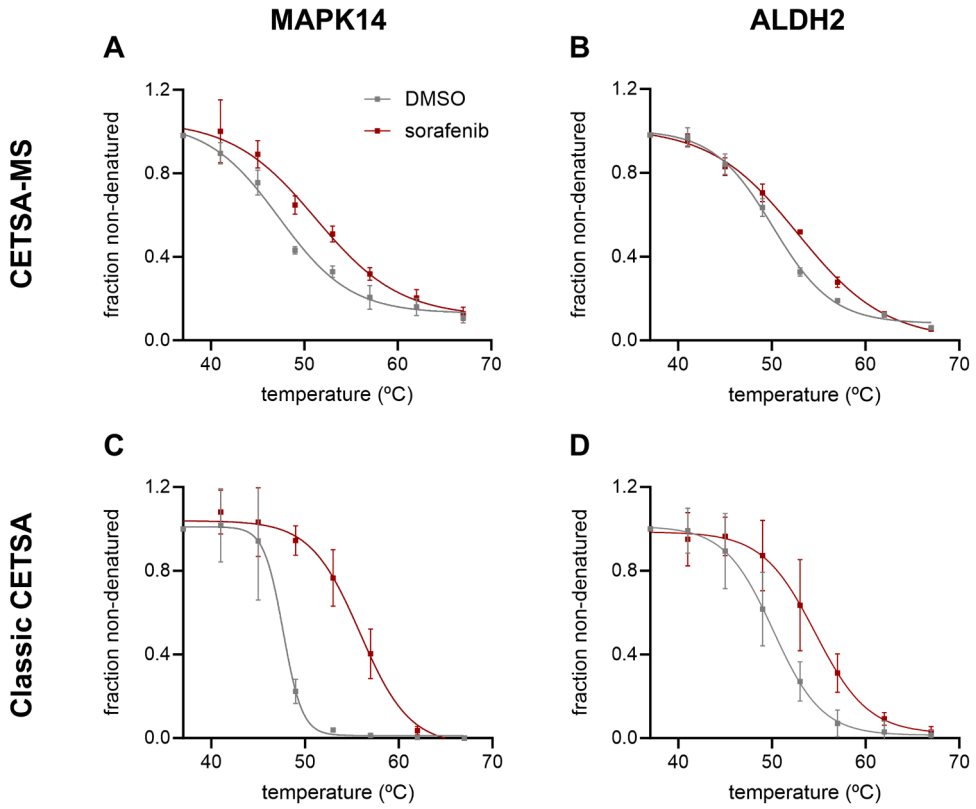

Fig. 2. Sorafenib effect on MAPK14 and ALDH2 thermal profiles determined by CETSA-MS and Classic CETSA using HepG2 lysates. HepG2 lysates were treated with 1 % (v/v) DMSO or sorafenib at 20 μM in 1 % (v/v) DMSO and heated at increasing temperatures. **(A, B)** Protein detection was performed by LC-MS/MS and protein quantification was monitored by iTRAQ. Error bars indicate the SD from $n = 4$ experiments. **(C, D)** Protein detection and quantification were performed by Capillary Western Blot. Error bars indicate the SD from $n = 3$ experiments. **(A)** $\Delta T_m = +4$ °C. **(B)** $\Delta T_m = +2$ °C. **(C)** $\Delta T_m = +8.2$ °C. **(D)** $\Delta T_m = +4.5$ °C. All experiments were performed as independent replicates. The data are normalized to the quantity of non-denatured fraction at the lowest temperature.

of approximately 10 (5.7 to 10.5 for HepG2S1 and 6 to 15.7 for HepG2S3) (Fig. 5A).

For the evaluation of ALDH2 activity in a biologically relevant system, we selected an activity assay to measure the generation of NADH by the endogenous ALDH2 in HepG2 cell lysates comparing both DMSO and sorafenib treatments. Both sorafenib-resistant cell lines showed decreased ALDH2 activity, with HepG2S1 and HepG2S3 cell lines presenting 7.7 % and 10.9 % of the NADH production observed in the corresponding parental cell line (HepG2B). No significant effect was observed after sorafenib treatment in the resistant cell lines. For the HepG2A cell line, a statistically significant inhibition of 31.1 % in NADH production was obtained in the presence of sorafenib, suggesting that sorafenib interferes with ALDH2 functionality. Disulfiram, a potent ALDH2 inhibitor [31], was used as positive control, revealing an inhibition of 91.9 % of ALDH2 activity, compared to the vehicle condition (Fig. 5B).

4. Discussion

Sorafenib is a well-studied multi-kinase inhibitor that has been used in the clinic for years but its complete range of targets is not yet fully characterized. CETSA-MS is an innovative approach to swiftly explore proteome-ligand interactions [15] and we applied it, for the first time, to study sorafenib engagement in an HCC cell line.

Several kinases, including Raf-1, B-Raf, VEGFR2, PDGFRβ, c-Kit, FLT-3 and MAPK14, have been described as sorafenib targets [2,5,7]. MAPK14 was confirmed to be engaged by sorafenib in our CETSA-MS study and as well in our Classic CETSA experiments (Fig. 2A and 2C). However, it was not possible to conclude on the engagement of the other established sorafenib targets. These proteins were either not identified in our CETSA-MS dataset or the corresponding quantification was obtained only for some temperature points, not enabling the correct melting curve determination. VEGFR2, PDGFRβ, c-Kit, and FLT-3 are membrane-spanning tyrosine kinase receptors and thus are expected to have poor solubility [32]. The Raf kinases Raf-1 and B-Raf, although typically present in the cytoplasm, are expressed at low levels in most cell types [30,33]. Additionally, when activated, these proteins can translocate to different cellular compartments, including the plasma membrane [34–36]. CETSA protocols are designed to deliberately remove the non-soluble fraction from CETSA samples and this leads to further reduction in the amount of protein available for MS detection. These factors might have impaired MS detection and quantification for these well-established sorafenib targets.

MAPK14 is part of the MAPK38 kinase family that regulates proliferation, differentiation, and apoptosis [37], and its downregulation promotes sorafenib resistance in HCC through abrogation of MAPK14-dependent MEK/ERK cascade activation [38–40]. The remaining 6 proteins identified as sorafenib targets in our CETSA-MS study (Fig. 1) are non-kinase proteins. In previous studies, other non-kinase proteins have been identified as sorafenib targets [14,41], opening the possibility that sorafenib might function by targeting other protein classes.

The majority of the proteins herein identified as potential sorafenib targets, namely ICAM1, TRM6, and PP6R1, have been described as being involved in HCC [42–46], suggesting that the potential mode-of-action of sorafenib may be related to the engagement with these targets; however, further confirmatory studies are required. To the extent of our knowledge, there is no described association of DYLT1 or RPCA1 in HCC.

ALDH2 was selected for further target validation due to its described

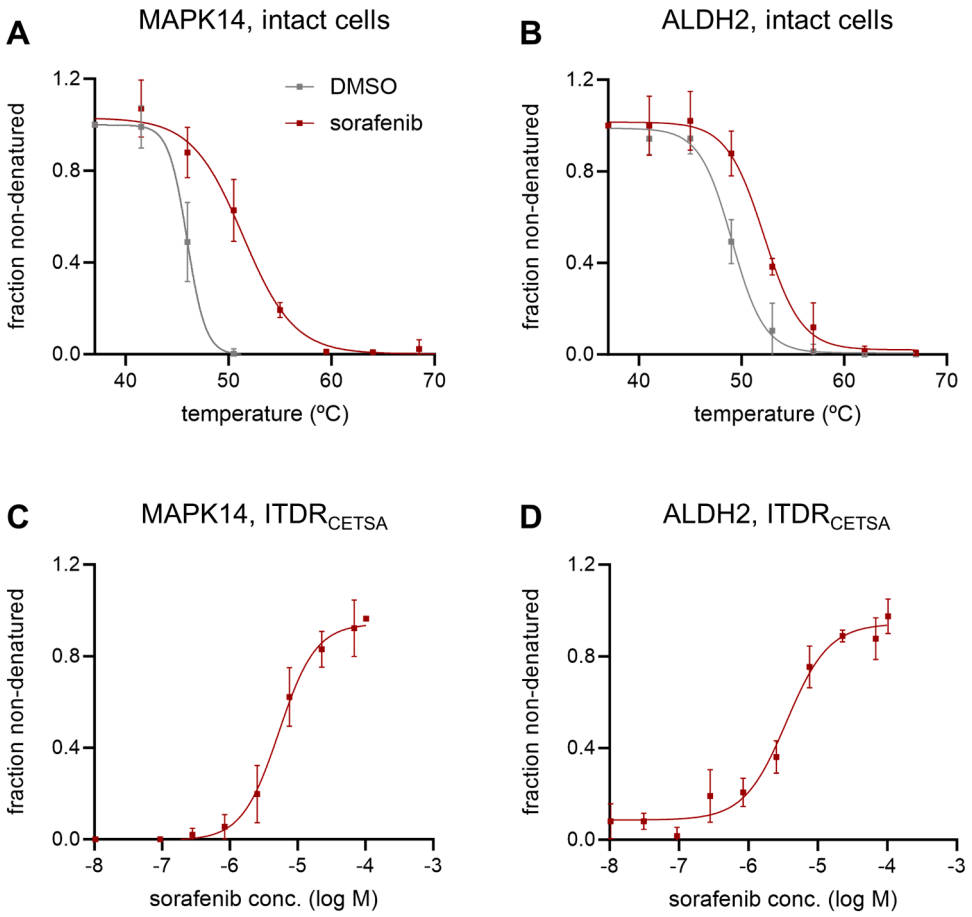

Fig. 3. Sorafenib effect on MAPK14 and ALDH2 thermal profiles determined by Classic CETSA using HepG2 intact cells and ITDR$_{CETSA}$ curves using HepG2 lysates. Protein detection and quantification were performed by Capillary Western Blot. **(A, B)** HepG2 intact cells were treated with 1 % (v/v) DMSO or sorafenib at 20 μM in 1 % (v/v) DMSO and heated at increasing temperatures. The data are normalized to the quantity of non-denatured fraction at the lowest temperature. Error bars indicate the SD from at least $n = 3$ experiments. **(C, D)** HepG2 lysates were treated with sorafenib in 1 % (v/v) DMSO over a range of concentrations. ITDR$_{CETSA}$ profiling was performed at 57 °C for MAPK14 and at 53 °C for ALDH2. The data are normalized to the quantity of non-denatured fraction at the highest compound concentration. Error bars indicate the SD from $n = 3$ experiments. **(A)** $\Delta T_m = +5.4$ °C. **(B)** $\Delta T_m = +3.1$ °C. **(C)** $EC_{50} = 5.3$ μM. **(D)** $EC_{50} = 3.5$ μM. All experiments were performed as independent replicates.

correlation with cancer and specifically with HCC. Some studies indicate that ALDH2 promotes proliferation [47] and, accordingly, that decreased ALDH2 expression suppress tumorigenesis [48,49]. However, it has also been described that ALDH2 downregulation, in both mRNA and protein expression, in several types of cancer is related to malignant phenotypes, tumor progression and adverse prognosis [22,50,51]. This has been vastly confirmed in HCC, with low expression of ALDH2 associated with development of the disease and poor prognosis in HCC patients [52–57]. Paradoxically, ALDH2 promotes the expression of several cancer stem biomarkers, leading to the proliferation, migration, and invasion of liver cancer stem cells [48].

Sorafenib engagement of ALDH2 observed by CETSA-MS (Fig. 2B) was confirmed by Classic CETSA in both HepG2 cell lysates (Fig. 2D) and intact cells (Fig. 3B), showing that sorafenib can diffuse across the cell membrane, reach, and bind ALDH2 at its final subcellular localization [58]. The concentration of sorafenib used in our CETSA experiments was relatively high compared to the potency of sorafenib determined for well-established targets [59]. However, it should be noted that it is common practice in CETSA assays to use compound concentrations in the micromolar range even when the expected affinities or IC_{50} of the compound under study is significantly lower [17,25,60]. This is critical to ensure that a clear change in the target thermal stability is observed in case of engagement and to compensate for the impact of temperature-induced equilibration occurring during the CETSA heat pulse that might induce a shift in the compound apparent potency [61]. Importantly, the phenotypically relevant sorafenib concentrations for several cell lines are in the micromolar range: IC_{50} of 5.5 μM for HepG2 and WRL-68 and 4.5 μM for Huh-7 [23], the same range of the concentration of sorafenib used in this study. Further studies, beyond the scope of the current work, would be required to characterize the affinity and mode of action of sorafenib targeting ALDH2 and assess engagement during treatment in patients.

In addition to CETSA experiments, binding of sorafenib to ALDH2 was validated using pure recombinant ALDH2 in DSF (Fig. 4A) and 1D ^{19}F NMR experiments (Fig. 4B) supporting a direct interaction independent of other binding partners.

The activity of the recombinant ALDH2 protein was assessed in a biochemical assay by monitoring NADH generation. ALDH2 activity was detected but no inhibition by the ALDH2 inhibitor disulfiram [31] was observed (data not shown), invalidating the results of the assay. Further assay optimization, testing alternative recombinant proteins or biochemical assays, can shed light on the potency of sorafenib inhibition. Nevertheless, we pursued with an activity assay in a biologically more relevant system, specifically directed to the endogenous ALDH2 in HepG2 cell lysates comparing both DMSO and sorafenib treatments, in which disulfiram inhibition was confirmed (91.9 %, Fig. 5B). Assessment of endogenous ALDH2 activity also enabled the comparison between HepG2 sorafenib-sensitive and sorafenib-resistant cell lines. Thus, we demonstrated that sorafenib reduced ALDH2 activity by approximately 30 % (Fig. 5B), showing that there is a functional role in

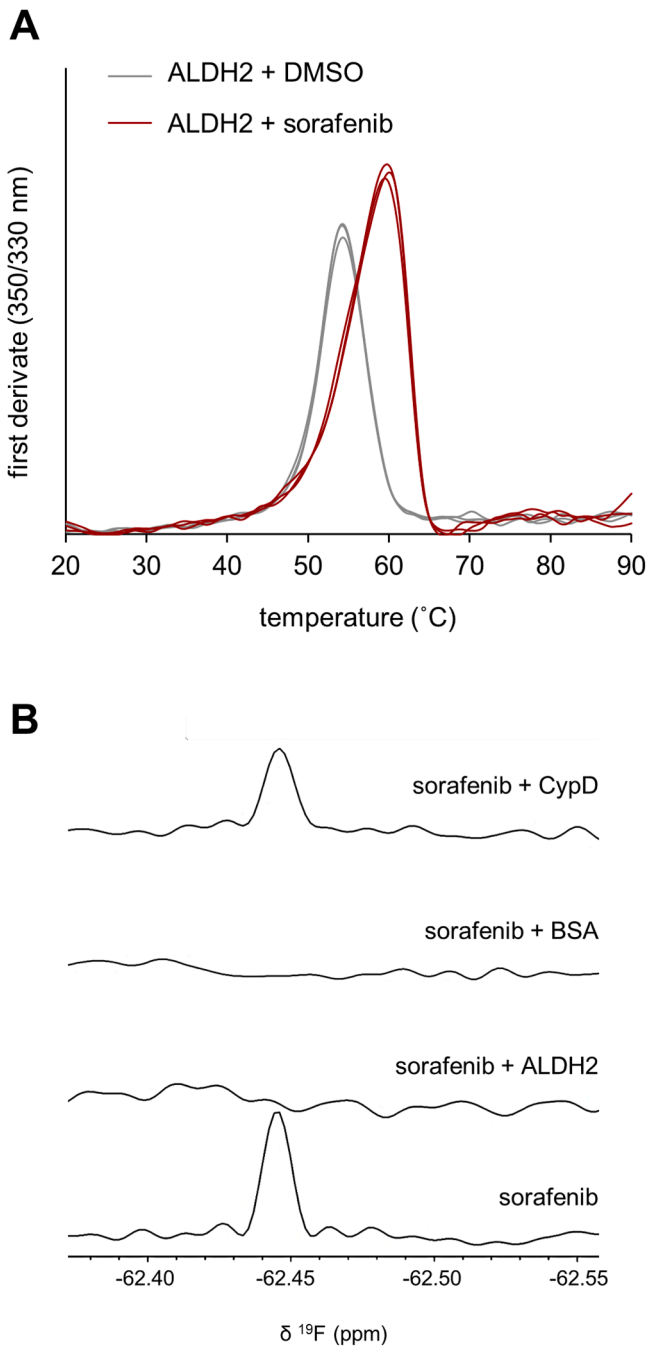

Fig. 4. Biophysical characterization of sorafenib binding to ALDH2. (A) ALDH2 melting profile in presence of 2 % DMSO (v/v) or sorafenib at 20 μM in 2 % DMSO (v/v) obtained in DSF experiments resulted in a $\Delta T_m = +5$ °C. Each sample was run in triplicate and the average T_m of the two samples was used to calculate the ΔT_m. **(B)** 1D ^{19}F NMR spectra of sorafenib at 5 μM, sorafenib at 5 μM plus 1 μM ALDH2, sorafenib at 5 μM plus 1 μM BSA (positive control) and sorafenib at 5 μM plus 1 μM CypD (negative control). All samples contained 10 μM TFA that was used to normalize signal intensity across the spectra.

sorafenib inhibition and also confirming target engagement. ALDH2 inhibition by sorafenib can play a role in HCC suppression by impairing the primary metabolic function of this mitochondrial enzyme that will lead to an excessive acetaldehyde accumulation [55,62,63]. The subsequent generation of ROS species would ultimately cause oxidative stress and induce apoptotic cancer cell death [64].

The role of ALDH2 in oncogenic signaling pathways is only partially understood but may also be relevant to the observed inhibition by sorafenib. A screening of more than 1000 clinical samples from more than 30 cancer types revealed that ALDH2 expression was positively related to immune and metastasis-related pathways, and a negative correlation was observed with proliferation-related pathways. These results suggest that ALDH2 might play multiple functions in distinct cancers [22]. Particularly in liver diseases like HCC, it has been observed that ALDH2 activates JAK-STAT-1 [65], AMPK [52] and MEK/ERK signaling pathways [66]. Although these mechanisms are not completely known, sorafenib may inhibit these signaling pathways through binding and/or inhibition of ALDH2.

The reduction in ALDH2 protein expression (Fig. 5A) and activity (Fig. 5B) in two sorafenib-HepG2 resistant cells may suggest that ALDH2 is downregulated in sorafenib-resistant cells. Although further studies are required to evaluate whether ALDH2 can be a potential sorafenib-resistance biomarker, the low protein levels observed in our study may support the functional role of sorafenib in ALDH2, since alteration in gene expression is a well described resistance characteristic [67]. Other factors may contribute to the low expression of this mitochondrial enzyme. Sorafenib has an inhibitory effect in the mitochondrial electron transport chain resulting in the collapse of mitochondrial membrane potential and consequent ATP production, ultimately leading to cell death due to ferroptosis [68,69]. The induction of sorafenib resistance in HCC cells is accompanied by high levels of mitophagy [70,71], a mitochondrial selective form of autophagy that is critical for mitochondrial homeostasis, as it eliminates damaged or dysfunctional mitochondria [72] potentially resulting in lower ALDH2 expression on these cells. In addition, MAPK14 inhibition by sorafenib could also be contributing to a downregulation of ALDH2 since it has been shown that MAPK38 activation induces ALDH2 expression in acute myeloid leukemia [73]. Finally, the low expression of ALDH2 in the sorafenib-resistant HepG2 cell lines, that display an invasive phenotype [23], is in accordance with the data that show a downregulation of ALDH2 in HCC human tissues and invasive HCC cell lines [52,56,57]. More studies are needed to understand if ALDH2 contributes to sorafenib primary and/or acquired resistance and if it can be used as a potential biomarker of sorafenib resistance in HCC patients.

With this study, novel insights on the identity of sorafenib-binding partners and potential cellular targets were acquired. Our results further characterize sorafenib polypharmacology showing that the drug binds to different targets, not only to kinase proteins. This knowledge can be important to comprehend the mode-of-action of sorafenib, its side effects as well as its resistance that is frequently acquired in advanced HCC patients. These new findings contribute to better explain how sorafenib acts as an anti-tumor therapeutic. Further studies for understanding the mode-of-action of sorafenib binding and inhibition of ALDH2 focusing on patient-derived samples in different stages of HCC development can be helpful to understand the role of ALDH2 in this context.

Author contributions

I. C. Ferreira, E. Torrejón, B. Abecasis, S. P. Rebelo and A. Bortoluzzi: conceptualization and writing—original draft. I. C. Ferreira and E. Torrejón: methodology. I. C. Ferreira, E. Torrejón, B. M. Alexandre and R. A. Gomes: experimental work. I. C. Ferreira, E. Torrejón and A. Bortoluzzi: formal analysis and visualization. I. C. Ferreira, E. Torrejón, S. P. Rebelo and A. Bortoluzzi: writing–original draft. I. C. Ferreira, E. Torrejón, B. Abecasis, B. M. Alexandre, R. A. Gomes, C. Verslype, J. van Pelt, A. Barbas, D. Simão, T. M. Bandeiras, S. P. Rebelo and A. Bortoluzzi: writing—review and editing. A. Barbas, T. M. Bandeiras, S. P. Rebelo and A. Bortoluzzi: funding acquisition. S. P. Rebelo and A. Bortoluzzi: supervision. All authors contributed to the article and approved the submitted version.

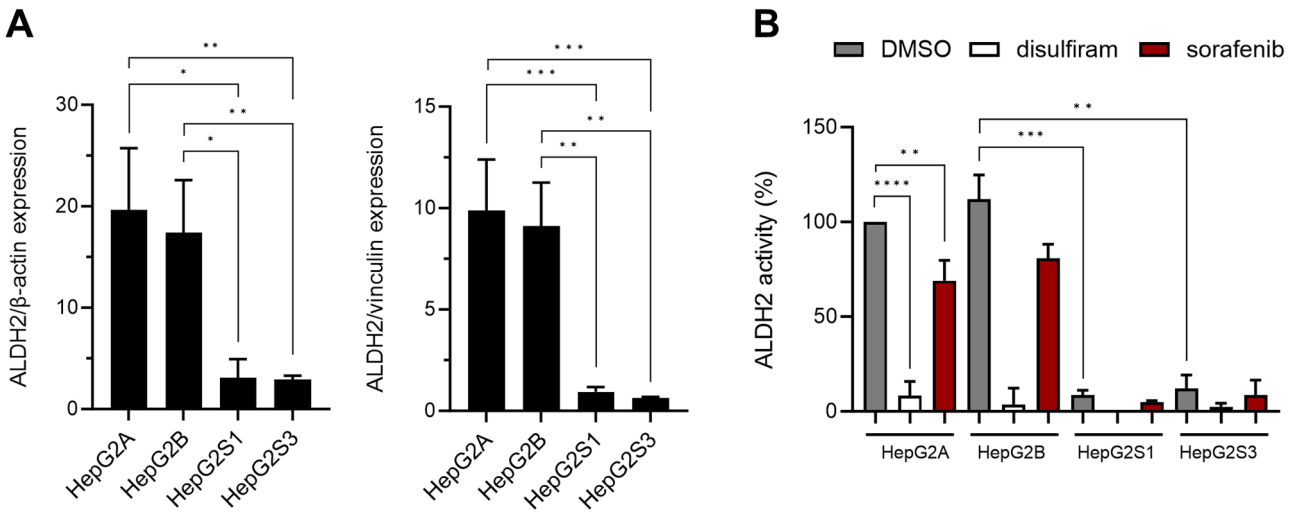

Fig. 5. Analysis of ALDH2 protein expression in HepG2 cell lines and sorafenib effect on ALDH2 activity. (A) HepG2 lysate concentration was adjusted to the same total protein concentration. Protein detection and quantification were performed by Capillary Western Blot. Relative ALDH2 expression was calculated by dividing ALDH2 protein quantification by the corresponding loading control (β-actin or vinculin) quantification for each sample. Error bars indicate the SD from at least $n = 3$ cell lysates **(B)** HepG2 lysates were incubated with 10 % DMSO, sorafenib or disulfiram at 100 μM in 10 % (v/v) DMSO. ALDH2 activity was determined by NADH production and the results refer to the timepoint of 30 min. The data are normalized to the activity of HepG2A with DMSO. HepG2A and HepG2B refer to sorafenib-sensitive cell lines; HepG2S1 and HepG2S3 refer to sorafenib-resistant cell lines. Error bars indicate the SD from at least $n = 2$ cell lysates **(A, B)** All experiments were performed as independent replicates. Unpaired *t*-tests were used to analyze the data. $^{*}p \leq 0.05$; $^{**}p \leq 0.01$; $^{***}p \leq 0.001$; $^{****}p \leq 0.0001$.

Funding

This work was supported by the Fundação para a Ciência e Tecnologia/Ministério da Ciência, Tecnologia e Ensino Superior (FCT/MCTES, Portugal) through national funds to iNOVA4Health (UIDB/04,462/2020 and UIDP/04,462/2020) and the Associate Laboratory LS4FUTURE (LA/P/0087/2020). The NMR data were acquired at CERMAX, ITQB-NOVA, Oeiras, Portugal with equipment funded by FCT, project AAC 01/SAICT/2016.

Declaration of competing interest

The authors declare the following financial interests/personal relationships which may be considered as potential competing interests:

Ana Barbas reports a relationship with Bayer Corporation that includes: employment. If there are other authors, they declare that they have no known competing financial interests or personal relationships that could have appeared to influence the work reported in this paper.

Acknowledgments

We thank UniMS–Mass Spectrometry Unit from ITQB/iBET (Oeiras, Portugal) for MS data acquisition, and particular to Patrícia Alves, Ana Guerreiro and Catarina Correia for discussions and technical support on mass spectrometry. We thank Pedro Lamosa for discussions and technical support on NMR. We also thank Joerg Bomke, Pedro Sousa, Carolina Cassona, Inês Isidro and Inês Carrondo for fruitful discussions.

Supplementary materials

Supplementary material associated with this article can be found, in the online version, at doi:10.1016/j.slasd.2024.100154.

References

[1] Llovet JM, Kelley RK, Villanueva A, Singal AG, Pikarsky E, Roayaie S, Lencioni R, Koike K, Zucman-Rossi J, Finn RS. Hepatocellular Carcinoma. Nat. Rev. Dis. Primer. 2021:7. https://doi.org/10.1038/s41572-020-00240-3.

[2] Llovet JM, Hilgard P, de Oliveira AC, Forner A, Zeuzem S, Galle PR, Häussinger D, Moscovici M. Sorafenib in advanced hepatocellular carcinoma. N. Engl. J. Med. 2008;359:378–90. https://doi.org/10.1056/NEJMoa0708857.

[3] Vogel A, Cervantes A, Chau I, Daniele B, Llovet JM, Meyer T, Nault J-C, Neumann U, Ricke J, Sangro B, et al. Hepatocellular carcinoma: ESMO clinical practice guidelines for diagnosis, treatment and follow-up. Ann. Oncol 2018;29: 238–55. https://doi.org/10.1093/annonc/mdy308.

[4] Wilhelm S, Chien D-S. BAY 43-9006: preclinical Data. Curr. Pharm. Des. 2002;8: 2255–7. https://doi.org/10.2174/1381612023393026.

[5] Wilhelm SM, Carter C, Tang L, Wilkie D, McNabola A, Rong H, Chen C, Zhang X, Vincent P, McHugh M, et al. BAY 43-9006 Exhibits Broad spectrum oral antitumor activity and targets the RAF/MEK/ERK Pathway and receptor tyrosine kinases involved in tumor progression and angiogenesis. Cancer Res 2004;64:7099–109. https://doi.org/10.1158/0008-5472.CAN-04-1443.

[6] Chang YS, Adnane J, Trail PA, Levy J, Henderson A, Xue D, Bortolon E, Ichetovkin M, Chen C, McNabola A, et al. Sorafenib (BAY 43-9006) Inhibits tumor growth and vascularization and induces tumor apoptosis and hypoxia in RCC Xenograft Models. Cancer Chemother. Pharmacol. 2007;59:561–74. https://doi.org/10.1007/s00280-006-0393-4.

[7] Liu L, Cao Y, Chen C, Zhang X, McNabola A, Wilkie D, Wilhelm S, Lynch M, Carter C. Sorafenib Blocks the RAF/MEK/ERK Pathway, inhibits tumor angiogenesis, and induces tumor cell apoptosis in hepatocellular carcinoma model PLC/PRF/5. Cancer Res 2006;66:11851–8. https://doi.org/10.1158/0008-5472.CAN-06-1377.

[8] Chapuy B, Schuelper N, Panse M, Dohm A, Hand E, Schroers R, Truemper L, Wulf GG. Multikinase Inhibitor sorafenib exerts cytocidal efficacy against non-hodgkin lymphomas associated with inhibition of MAPK14 and AKT Phosphorylation. Br. J. Haematol. 2011;152:401–12. https://doi.org/10.1111/j.1365-2141.2010.08526.x.

[9] Coriat R, Nicco C, Chéreau C, Mir O, Alexandre J, Ropert S, Weill B, Chaussade S, Goldwasser F, Batteux F. Sorafenib-induced hepatocellular carcinoma cell death depends on reactive oxygen species production in vitro and in vivo. Mol. Cancer Ther. 2012;11:2284–93. https://doi.org/10.1158/1535-7163.MCT-12-0093.

[10] Lachaier E, Louandre C, Godin C, Saidak Z, Baert M, Diouf M, Chauffert B, Galmiche A. Sorafenib induces ferroptosis in human cancer cell lines originating from different solid tumors. Anticancer Res 2014;34:6417–22.

[11] Cervello M, Bachvarov D, Lampiasi N, Cusimano A, Azzolina A, McCubrey JA, Montalto G. Molecular mechanisms of sorafenib action in liver cancer cells. Cell Cycle 2012;11:2843–55. https://doi.org/10.4161/cc.21193.

[12] Contreras L, Rodríguez-Gil A, Muntané J, De La Cruz J. Broad transcriptomic impact of sorafenib and its relation to the antitumoral properties in liver cancer cells. Cancers (Basel) 2022;14:1204. https://doi.org/10.3390/cancers14051204.

[13] Hou C, Guo D, Yu X, Wang S, Liu T. TMT-based proteomics analysis of the anti-hepatocellular carcinoma effect of combined dihydroartemisinin and sorafenib. Biomed. Pharmacother. 2020;126:109862. https://doi.org/10.1016/j.biopha.2020.109862.

[14] Li Y, Meng Q, Wang P, Liu X, Fu Q, Xie Y, Zhou Y, Qi X, Huang N. Identification of PDE6D as a Potential target of sorafenib via PROTAC Technology. BioRxiv Prepr 2020. https://doi.org/10.1101/2020.05.06.079947.

[15] Molina DM, Jafari R, Ignatushchenko M, Seki T, Larsson EA, Dan C, Sreekumar L, Cao Y, Nordlund P. Monitoring drug target engagement in cells and tissues using

the cellular thermal shift assay. Science 2013;341:84–7. https://doi.org/10.1126/science.1233606.
[16] Brandts JF, Lin LN. Study of Strong to ultratight protein interactions using differential scanning calorimetry. Biochemistry 1990;29:6927–40. https://doi.org/10.1021/bi00481a024.
[17] Savitski MM, Reinhard FBM, Franken H, Werner T, Savitski MF, Eberhard D, Molina DM, Jafari R, Dovega RB, Klaeger S, et al. Tracking cancer drugs in living cells by thermal profiling of the proteome. Science 2014;346:1255784. https://doi.org/10.1126/science.1255784.
[18] Klyosov AA, Rashkovetsky LG, Tahir MK, Keung W-M. Possible role of liver cytosolic and mitochondrial aldehyde dehydrogenases in acetaldehyde metabolism. Biochemistry 1996;35:4445–56. https://doi.org/10.1021/bi9521093.
[19] Gao J, Hao Y, Piao X, Gu X. Aldehyde Dehydrogenase 2 as a therapeutic target in oxidative stress-related diseases: post-translational modifications deserve more attention. Int. J. Mol. Sci. 2022;23:2682. https://doi.org/10.3390/ijms23052682.
[20] Chen C-H, Ferreira JCB, Gross ER, Mochly-Rosen D. Targeting aldehyde dehydrogenase 2: new therapeutic opportunities. Physiol. Rev. 2014;94:1–34. https://doi.org/10.1152/physrev.00017.2013.
[21] Zhang H, Fu L. The role of ALDH2 in tumorigenesis and tumor progression: targeting ALDH2 as a potential cancer treatment. Acta Pharm. Sin. B 2021;11:1400–11. https://doi.org/10.1016/j.apsb.2021.02.008.
[22] Ma B, Liu Z, Xu H, Liu L, Huang T, Meng L, Wang L, Zhang Y, Li L, Han X. Molecular characterization and clinical relevance of ALDH2 in human cancers. Front. Med. 2022;8. https://doi.org/10.3389/fmed.2021.832605.
[23] Van Malenstein H, Dekervel J, Verslype C, Van Cutsem E, Windmolders P, Nevens F, Van Pelt J. Long-term exposure to sorafenib of liver cancer cells induces resistance with epithelial-to-mesenchymal transition, increased invasion and risk of rebound growth. Cancer Lett 2013;329:74–83. https://doi.org/10.1016/j.canlet.2012.10.021.
[24] Chernobrovkin AL, Lengqvist J, Körner CC, Amadio D, Friman T, Molina DM. In-Depth Characterization of Staurosporine Induced Proteome Thermal Stability Changes. BioRxiv Prepr 2020. https://doi.org/10.1101/2020.03.13.990606.
[25] Friman T, Chernobrovkin A, Molina DM, Arnold L. CETSA MS profiling for a comparative assessment of FDA approved antivirals repurposed for COVID-19 therapy identifies TRIP13 as a remdesivir off-target. SLAS Discov 2021;26:336–44. https://doi.org/10.1177/2472555220973597.
[26] Childs D, Kurzawa N, Franken H, Doce C, Savitski M, Huber W. Analyze Thermal Proteome Profiling (TPP) Experiments 2019.
[27] Grossi V, Liuzzi M, Murzilli S, Martelli N, Napoli A, Ingravallo G, Del Rio A, Simone C. Sorafenib inhibits P38α Activity in colorectal cancer cells and synergizes with the DFG-in Inhibitor SB202190 to increase apoptotic response. Cancer Biol. Ther. 2012;13:1471–81. https://doi.org/10.4161/cbt.22254.
[28] Gossert AD, Jahnke W. NMR in Drug discovery: a Practical guide to identification and validation of ligands interacting with biological macromolecules. Prog. Nucl. Magn. Reson. Spectrosc. 2016;97:82–125. https://doi.org/10.1016/j.pnmrs.2016.09.001.
[29] Dalvit C, Vulpetti A. Ligand-based fluorine nmr screening: principles and applications in drug discovery projects. J. Med. Chem. 2019;62:2218–44. https://doi.org/10.1021/acs.jmedchem.8b01210.
[30] Shi J-H, Chen J, Wang J, Zhu Y-Y, Wang Q. Binding interaction of sorafenib with bovine serum albumin: spectroscopic methodologies and molecular docking. Spectrochim. Acta. A. Mol. Biomol. Spectrosc. 2015;149:630–7. https://doi.org/10.1016/j.saa.2015.04.034.
[31] Vallari RC, Pietruszko R. Human aldehyde dehydrogenase: mechanism of inhibition of disulfiram. Science 1982;216:637–9. https://doi.org/10.1126/science.7071604.
[32] Robinson DR, Wu Y-M, Lin S-F. The protein tyrosine kinase family of the human genome. Oncogene 2000;19:5548–57. https://doi.org/10.1038/sj.onc.1203957.
[33] Kulak NA, Pichler G, Paron I, Nagaraj N, Mann MMinimal. Encapsulated proteomic-sample processing applied to copy-number estimation in eukaryotic Cells. Nat. Methods 2014;11:319–24. https://doi.org/10.1038/nmeth.2834.
[34] Anderson DJ, Durieux JK, Song K, Alvarado R, Jackson PK, Hatzivassiliou G, Ludlam MJC. Live-Cell microscopy reveals small molecule inhibitor effects on MAPK pathway dynamics. PLoS ONE 2011;6:e22607. https://doi.org/10.1371/journal.pone.0022607.
[35] Nan X, Collisson EA, Lewis S, Huang J, Tamgüney TM, Liphardt JT, McCormick F, Gray JW, Chu S. Single-Molecule superresolution imaging allows quantitative analysis of RAF multimer formation and signaling. Proc. Natl. Acad. Sci 2013;110:18519–24. https://doi.org/10.1073/pnas.1318188110.
[36] Terrell EM, Morrison DK. Ras-mediated activation of the raf family kinases. Cold Spring Harb. Perspect. Med. 2019;9:a033746. https://doi.org/10.1101/cshperspect.a033746.
[37] Cargnello M, Roux PP. Activation and Function of the MAPKs and Their Substrates, the MAPK-Activated Protein Kinases. Microbiol. Mol. Biol. Rev. 2011;75:50–83. https://doi.org/10.1128/MMBR.00031-10.
[38] Avila M, Berasain C. Making sorafenib irresistible: in Vivo screening for mechanisms of therapy resistance in hepatocellular carcinoma hits on mapk14. Hepatology 2015;61:1755–7. https://doi.org/10.1002/hep.27739.
[39] Wan Z, Liu T, Wang L, Wang R, Zhang H. MicroRNA-216a-3p promotes sorafenib sensitivity in hepatocellular carcinoma by downregulating MAPK14 expression. Aging 2020;12:18192–208. https://doi.org/10.18632/aging.103670.
[40] Fritz V, Malek L, Gaza A, Wormser L, Appel M, Kremer AE, Thasler WE, Siebler J, Neurath MF, Hellerbrand C, et al. Combined de-repression of chemoresistance associated mitogen-activated protein kinase 14 and activating transcription factor 2 by loss of microRNA-622 in hepatocellular carcinoma. Cancers (Basel) 2021;13:1183. https://doi.org/10.3390/cancers13051183.
[41] Lin X, Huang X-P, Chen G, Whaley R, Peng S, Wang Y, Zhang G, Wang SX, Wang S, Roth BL, et al. Life beyond kinases: structure-based discovery of sorafenib as nanomolar antagonist of 5-HT receptors. J. Med. Chem. 2012;55:5749–59. https://doi.org/10.1021/jm300338m.
[42] Cheng Z, Li X, Ding J. Characteristics of liver cancer stem cells and clinical correlations. Cancer Lett 2016;379:230–8. https://doi.org/10.1016/j.canlet.2015.07.041.
[43] Benedicto A, Romayor I, Arteta B. Role of liver ICAM-1 in metastasis. Oncol. Lett. 2017;14:3883–92. https://doi.org/10.3892/ol.2017.6700.
[44] Wang Y, Huang Q, Deng T, Li B-H, Ren X-Q. Clinical Significance of TRMT6 in hepatocellular carcinoma: a bioinformatics-based study. Med. Sci. Monit. 2019;25:3894–901. https://doi.org/10.12659/MSM.913556.
[45] Ohama T. The multiple functions of protein phosphatase 6. Biochim. Biophys. Acta BBA - Mol. Cell Res. 2019;1866:74–82. https://doi.org/10.1016/j.bbamcr.2018.07.015.
[46] Ye Y, Liu M, Wu F, Ou S, Wang W, Fei J, Xie F, Bai L. TRMT6 promotes hepatocellular carcinoma progression through the PI3K/AKT Signaling Pathway. Eur. J. Med. Res. 2023;28:48. https://doi.org/10.1186/s40001-022-00951-1.
[47] Moreb JS, Ucar D, Han S, Amory JK, Goldstein AS, Ostmark B, Chang L-J. The enzymatic activity of human aldehyde dehydrogenases 1A2 and 2 (ALDH1A2 and ALDH2) Is Detected by Aldefluor, Inhibited by Diethylaminobenzaldehyde and Has significant effects on cell proliferation and drug resistance. Chem. Biol. Interact. 2012;195:52–60. https://doi.org/10.1016/j.cbi.2011.10.007.
[48] Chen L, Wu M, Ji C, Yuan M, Liu C, Yin Q. Silencing Transcription Factor FOXM1 represses proliferation, migration, and invasion while inducing apoptosis of liver cancer stem cells by regulating the expression of ALDH2. IUBMB Life 2020;72:285–95. https://doi.org/10.1002/iub.2166.
[49] Wang W, Wang J, Liu S, Ren Y, Wang J, Liu S, Cui W, Jia L, Tang X, Yang J, et al. An EHMT2/NFYA-ALDH2 Signaling Axis Modulates the RAF Pathway to Regulate Paclitaxel Resistance in Lung Cancer. Mol. Cancer 2022;21:106. https://doi.org/10.1186/s12943-022-01579-9.
[50] Li K, Guo W, Li Z, Wang Y, Sun B, Xu D, Ling J, Song H, Liao Y, Wang T, et al. ALDH2 repression promotes lung tumor progression via accumulated acetaldehyde and DNA damage. Neoplasia 2019;21:602–14. https://doi.org/10.1016/j.neo.2019.03.008.
[51] Yao S, Yin X, Chen T, Chen W, Zuo H, Bi Z, Zhang X, Jing Y, Pang L, Cheng H. Exploring ALDH2 Expression and immune infiltration in HNSC and its correlation of prognosis with gender or alcohol intake. Sci. Rep. 2022;12:2504. https://doi.org/10.1038/s41598-022-06244-1.
[52] Hou G, Chen L, Liu G, Li L, Yang Y, Yan H, Zhang H, Tang J, Yang YC, Lin X, et al. Aldehyde Dehydrogenase-2 (ALDH2) Opposes Hepatocellular Carcinoma Progression by Regulating AMP-Activated Protein Kinase Signaling in Mice. Hepatology 2017;65:1628–44. https://doi.org/10.1002/hep.29006.
[53] Jin S, Chen J, Chen L, Histen G, Lin Z, Gross S, Hixon J, Chen Y, Kung C, Chen Y, et al. ALDH2(E487K) mutation increases protein turnover and promotes murine hepatocarcinogenesis. Proc. Natl. Acad. Sci 2015;112:9088–93. https://doi.org/10.1073/pnas.1510757112.
[54] Chen X, Legrand AJ, Cunniffe S, Hume S, Poletto M, Vaz B, Ramadan K, Yao D, Dianov GL. Interplay between Base Excision Repair Protein XRCC1 and ALDH2 predicts overall survival in lung and liver cancer patients. Cell. Oncol. 2018;41:527–39. https://doi.org/10.1007/s13402-018-0390-8.
[55] Seo W, Gao Y, He Y, Sun J, Xu H, Feng D, Park SH, Cho Y-E, Guillot A, Ren T, et al. ALDH2 deficiency promotes alcohol-associated liver cancer by activating oncogenic pathways via oxidized dna-enriched extracellular vesicles. J. Hepatol. 2019;71:1000–11. https://doi.org/10.1016/j.jhep.2019.06.018.
[56] Yao S, Yin X, Chen T, Chen W, Zuo H, Bi Z, Zhang X, Jing Y, Pang L, Cheng H. ALDH2 Is a prognostic biomarker and related with immune infiltrates in HCC. Am. J. Cancer Res. 2021;11:5319–37.
[57] Singh P, Gurung R, Sultan A, Dohare R. Understanding the role of adipokines and adipogenesis family in hepatocellular carcinoma. Egypt. J. Med. Hum. Genet. 2023:24. https://doi.org/10.1186/s43042-023-00401-5.
[58] Ehrig T, Bosron WF, Li T-K. Alcohol and Aldehyde Dehydrogenase. Alcohol Alcohol 1990;25:105–16. https://doi.org/10.1093/oxfordjournals.alcalc.a044985.
[59] Wilhelm S, Carter C, Lynch M, Lowinger T, Dumas J, Smith RA, Schwartz B, Simantov R, Kelley S. Discovery and development of sorafenib: a multikinase inhibitor for treating cancer. Nat. Rev. Drug Discov. 2006;5:835–44. https://doi.org/10.1038/nrd2130.
[60] Franken H, Mathieson T, Childs D, Sweetman GMA, Werner T, Tögel I, Doce C, Gade S, Bantscheff M, Drewes G, et al. Thermal proteome profiling for unbiased identification of direct and indirect drug targets using multiplexed quantitative mass spectrometry. Nat. Protoc. 2015;10:1567–93. https://doi.org/10.1038/nprot.2015.101.
[61] Seashore-Ludlow B, Axelsson H, Lundbäck T. Perspective on CETSA Literature: toward more quantitative data interpretation. SLAS Discov 2020;25:118–26. https://doi.org/10.1177/2472555219884524.
[62] Chang JS, Hsiao J-R, Chen C-H. ALDH2 Polymorphism and alcohol-related cancers in asians: a public health perspective. J. Biomed. Sci. 2017:24. https://doi.org/10.1186/s12929-017-0327-y.
[63] Tsai M-C, Yang S-S, Lin C-C, Wang W-L, Hsu Y-C, Chen Y-S, Hu J-T, Lin JY, Yu M-L, Lin C-W. Association of Heavy Alcohol Intake and *ALDH2* Rs671 polymorphism with hepatocellular carcinoma and mortality in patients with hepatitis B Virus–related cirrhosis. JAMA Netw. Open 2022;5:e2223511. https://doi.org/10.1001/jamanetworkopen.2022.23511.
[64] Juan CA, Pérez De La Lastra JM, Plou FJ, Pérez-Lebeña E. The chemistry of reactive oxygen species (ROS) revisited: outlining Their Role in Biological macromolecules

(DNA, Lipids and Proteins) and Induced Pathologies. Int. J. Mol. Sci. 2021;22: 4642. https://doi.org/10.3390/ijms22094642.
[65] Wu Y, Yao Y, Tao L, Wang S, Hu Y, Li L, Hu S, Meng X, Yang D-S, Li H, et al. The role of acetaldehyde dehydrogenase 2 in the pathogenesis of liver diseases. Cell. Signal. 2023;102:110550. https://doi.org/10.1016/j.cellsig.2022.110550.
[66] Zhang H, Xue L, Li B, Zhang Z, Tao S. Vitamin D protects against alcohol-induced Liver Cell Injury Within an NRF2–ALDH2 Feedback Loop. Mol. Nutr. Food Res. 2019;63:1801014. https://doi.org/10.1002/mnfr.201801014.
[67] Emran TB, Shahriar A, Mahmud AR, Rahman T, Abir MH, Siddiquee MohdF-R, Ahmed H, Rahman N, Nainu F, Wahyudin E;, et al. Multidrug Resistance in Cancer: understanding Molecular Mechanisms, Immunoprevention and Therapeutic Approaches. Front. Oncol. 2022;12:891652. https://doi.org/10.3389/fonc.2022.891652.
[68] Zhang C, Liu Z, Bunker E, Ramirez A, Lee S, Peng Y, Tan A-C, Eckhardt SG, Chapnick DA, Liu X. Sorafenib Targets the mitochondrial electron transport chain complexes and ATP Synthase to Activate the PINK1–parkin pathway and modulate cellular drug response. J. Biol. Chem. 2017;292:15105–20. https://doi.org/10.1074/jbc.M117.783175.
[69] Li Y, Xia J, Shao F, Zhou Y, Yu J, Wu H, Du J, Ren X. Sorafenib induces mitochondrial dysfunction and exhibits synergistic effect with cysteine depletion by promoting HCC Cells ferroptosis. Biochem. Biophys. Res. Commun. 2021;534: 877–84. https://doi.org/10.1016/j.bbrc.2020.10.083.
[70] Wu H, Wang T, Liu Y, Li X, Xu S, Wu C, Zou H, Cao M, Jin G, Lang J, et al. Mitophagy promotes sorafenib resistance through hypoxia-inducible ATAD3A dependent axis. J. Exp. Clin. Cancer Res. 2020;39:274. https://doi.org/10.1186/s13046-020-01768-8.
[71] Zhang S, Wang Y, Cao Y, Wu J, Zhang Z, Ren H, Xu X, Kaznacheyeva E, Li Q, Wang G. Inhibition of the PINK1-Parkin Pathway enhances the lethality of sorafenib and regorafenib in hepatocellular carcinoma. Front. Pharmacol. 2022;13: 851832. https://doi.org/10.3389/fphar.2022.851832.
[72] Youle RJ, Narendra DP. Mechanisms of mitophagy. Nat. Rev. Mol. Cell Biol. 2011; 12:9–14. https://doi.org/10.1038/nrm3028.
[73] Kudaravalli S, Den Hollander P, Mani SA. Role of P38 MAP kinase in cancer stem cells and metastasis. Oncogene 2022;41:3177–85. https://doi.org/10.1038/s41388-022-02329-3.